Article

Copper-Based Intermetallic Electride Catalyst for Chemoselective Hydrogenation Reactions

Tian-Nan Ye, Yangfan Lu, Jiang Li, Takuya Nakao, Hongsheng Yang, Tomofumi Tada, Masaaki Kitano, and Hideo Hosono

Just Accepted

Copper-Based Intermetallic Electride Catalyst for Chemoselective Hydrogenation Reactions

Tian-Nan Ye,[1,2†] Yangfan Lu,[1,2†] Jiang Li,[1,2] Takuya Nakao,[3] Hongsheng Yang,[1,2] Tomofumi Tada,[1] Masaaki Kitano,[1] Hideo Hosono[1,2,3*]

[1]Materials Research Center for Element Strategy, Tokyo Institute of Technology, 4259 Nagatsuta, Midori-ku, Yokohama 226-8503, Japan

[2]ACCEL, Japan Science and Technology Agency, 4-1-8 Honcho, Kawaguchi, Saitama 332-0012, Japan

[3]Laboratory for Materials and Structures, Tokyo Institute of Technology, 4259 Nagatsuta, Midori-ku, Yokohama 226-8501, Japan

ABSTRACT: The development of transition metal intermetallic compounds, in which active sites are incorporated in lattice frameworks, has great potential for modulating the local structure and the electronic properties of active sites, and enhancing the catalytic activity and stability. Here we report that a new copper-based intermetallic electride catalyst, $LaCu_{0.67}Si_{1.33}$, in which Cu sites activated by anionic electrons with low work function are atomically dispersed in the lattice framework and affords selective hydrogenation of nitroarenes with above 40-times higher turnover frequencies (TOFs up to 5084 h^{-1}) than well-studied metal-loaded catalysts. Kinetic analysis utilizing isotope effect reveals that the cleavage of the H–H bond is the rate-determining step. Surprisingly, the high carrier density and low work function (LWF) properties of $LaCu_{0.67}Si_{1.33}$ enable the activation of hydrogen molecules with extreme low activation energy (E_a = 14.8 kJ·mol^{-1}). Furthermore, preferential adsorption of nitroarenes via a nitro group is achieved by high oxygen affinity of $LaCu_{0.67}Si_{1.33}$ surface, resulting in high chemoselectivity. The present efficient catalyst can further trigger the hydrogenation of other oxygen-containing functional groups such as aldehydes and ketones with high activities. These findings demonstrate that the transition metals incorporated in the specific lattice site function as catalytically active centers and surpass the conventional metal-loaded catalysts in activity and stability.

1.INTRODUCTION

In heterogeneous catalysts, supported metal nanostructures have been studied as the most universal platform for hydrogenation reactions.[1] It was discussed that the low-coordinated metal sites serve as active centers and smaller particles are required for enhancing catalytic activity.[2] Single atom catalyst systems have therefore been drawing considerable attention to maximize the utilization of atom efficiency.[3] However, such atomically dispersed metals with large surface free energy are often not stable enough on the support surface and may aggregate during reaction processes, resulting in a drastic degradation of catalytic activity.[4] To overcome these critical issues, chemical industry is currently exploring robust catalysts in which support itself can trap the single active metals in its lattice frameworks so that to achieve both of high activity and stability.

Recently, electride materials, compounds in which electrons serve as anions,[5] were applied for various molecular activation and chemical reactions, such as carbon dioxide splitting, hydrotrifluoromethylation of alkenes and alkynes, and chemoselective reduction and oxidation of ketones.[6] One of the intrinsic characteristics of the electride catalysts is their strong electron donating ability associated with the high electron density and a low work function (LWF) properties.[7] For instance, the recently reported ammonia synthesis catalyst support, $[Ca_{24}Al_{28}O_{64}]^{4+}(e^-)_4$ (C12A7:e$^-$), possesses much higher carrier density (ca. 10^{-21} cm^{-3}) than well-studied insulating supports, such as Al_2O_3 and CaO.[8] The work function (Φ_{WF}) of C12A7:e$^-$, on the other hand, is as low as ca. 2.4 eV, which is comparable to that of alkali and alkali earth metals.[9] As a result, highly activated electrons can be efficiently transferred into the lowest unoccupied molecular orbitals (LUMOs) of absorbed molecules. Due to the anti-bonding characters of LUMOs states, such electron donation significantly weakens the chemical bonds of the absorbed molecules, and enables molecular dissociation with lower activation energy.[10] The active sites of the electride material based catalysts therefore exhibit high catalytic activity, even when the surface area is one order of magnitude lower than those of traditional catalysts.[11] However, the most of electride materials still need to load catalytic active metals because the electride itself cannot work as a catalyst without supported metals. Furthermore, most of electride materials reported to date cannot be applied to some liquid processes due to the sensitivity to moisture, which restricts the reaction conditions.

In the course of our development for new catalysts with above in mind, we have focused on three key characteristics to ameliorate their general versatility. First, the catalyst should be chemically stable under the reaction conditions. Second, the active metals should be involved in the lattice framework to avoid aggregation and/or leaching. Finally, the catalyst should host both high carrier density and low work function features so that to activate substrate molecules under mild conditions. Recently, intermetallic compounds have been regarded as a new class of catalysts for various chemical reactions.[12] We can precisely control the electronic and geometric structure at an

atomic level in intermetallic compounds.[13] Moreover, the lattice framework of intermetallic compounds can isolate contiguous active sites, preventing sinter and leaching problems. To date, although many binary intermetallic catalysts have been employed,[14] limited success has been achieved in ternary intermetallic catalysts especially containing both rare earth and transition metals. Ternary intermetallic compounds composed of rare earth, transition metal, and p-block element (RTX intermetallic compounds) have unique electrical and magnetic properties, and can store hydrogen effectively in the lattice.[15] Therefore, the transition metal site in RTX compounds is expected to show unique catalytic properties because its electronic and geometric structure is largely different from those of single- and binary-metal system.

Herein we report that a new Cu based intermetallic electride, $LaCu_{0.67}Si_{1.33}$, is chemically stable and efficient for various hydrogenation reactions. $LaCu_{0.67}Si_{1.33}$ hosts strong electron donation ability because of its low work function and encourages dissociation of hydrogen molecules with reduced activation energy. $LaCu_{0.67}Si_{1.33}$ was found to afford selective hydrogenation with various functionalized groups, and we will discuss the co-existence of strong electron donating ability and Cu sites as possible key ingredients to realize such outstanding catalytic activity.

2. EXPERIMENTAL SECTION

Sample preparation. $LaCu_{0.67}Si_{1.33}$ and LaSi powder were directly synthesized by arc-melting lanthanum, copper and silicon ingots with a stoichiometric ratio under an argon atmosphere. The ingot obtained was silver colored and was ground using an agate motor. $LaCu_{0.67}Si_{1.33}H_{0.3}$ powder was obtained from the $LaCu_{0.67}Si_{1.33}$ catalyst annealed at 400 °C under H_2 gas flow for 24 h.

Physical property measurements. The electronic transport properties, magnetic susceptibility and heat capacity measurements were conducted using a physical property measurement system (PPMS) and a SQUID vibrating sample magnetometer (SVSM) from Quantum Design. The work function of $LaCu_{0.67}Si_{1.33}$ was measured using photoelectron yield spectroscopy (PYS). The base pressure of the PYS chamber was better than 10^{-7} Pa.

General procedure for the catalytic hydrogenation reactions. All reactions were conducted in a 25 mL stainless steel autoclave fitted with a glass mantle, a 60-bar manometer, and a magnetic stirrer. In a typical reaction, 0.5 mmol of substrates and 50 mg of catalyst were mixed in 5 mL of solvent. The autoclave was then flushed three times with H_2, pressurized with H_2 (3.0 MPa), and reactions were performed in the autoclave at 80 °C. The products were analysed using gas chromatography (GC) with an external standard of n-hexadecane and the identity of the products was further confirmed from gas chromatography-mass spectrometry (GC-MS) measurements. TOF was calculated from the reaction rate at low conversion level derived by the number of Cu atoms exposed to the catalyst surface (Eqs. 1 and 2):

$$TOF = n_0C/tn_{catalyst}, \qquad (1)$$

$$n_{cat} = m_{cat}N_{Cu\,sites}/N_A, \qquad (2)$$

where n_0 is the initial moles of substrate, C is the conversion of substrate at reaction time t, n_{cat} is the moles of Cu atoms exposed on the surface, m_{cat} is the weight of the catalyst, N_{Cu}

sites is the amount of exposed Cu atoms per gram of catalyst, and N_A is Avogadro's constant.

Sample Characterization. Powder XRD patterns were collected on a Bruker D8 Advance diffractometer with Cu Kα radiation at room temperature. The Brunauer-Emmett-Teller specific surface areas of the samples were determined from nitrogen adsorption–desorption isotherms measured at -196 °C using an automatic gas-adsorption instrument (BELSORP-mini II, MiccrotracBEL) after evacuation of the samples at 150 °C. H_2-temperature-programmed desorption (H_2-TPD) profiles were measured with a BELCAT-A instrument (MiccrotracBEL, Japan). 500 mg samples were pretreated in He (30 mL·min^{-1}) at 323 K for 30 min and then cooled to room temperature. The same He gas was employed at a flow rate of 30 mL·min^{-1} and a heating rate of 10 K·min^{-1} from room temperature to 1173 K. The H_2 desorption was monitored by a thermal conductivity detector (TCD) and mass spectrometer (Bell Mass, MiccrotracBEL, Japan).

DFT calculations. DFT calculations were performed using the Vienna *Ab initio* Simulation Package (VASP 5.2).[16] The exchange-correlation functional in DFT was described using the Perdew-Burke-Ernzerhof (PBE)-type generalized gradient approximation (GGA).[17] The core electrons are handled in the projector augmented wave method, and valence electrons are represented with wave functions based on plane waves.[18] A cut-off energy of 400 eV and 16×16×6 of Monkhorst-Pack k-point meshes were used for band structure calculations of stoichiometric LaCuSi.[19] For the electronic structure calculations of disordered $LaCu_{0.67}Si_{1.33}$, a 2×2×3 supercell of LaCuSi was adopted and eight Cu atoms were replaced with Si atoms to form $La_{12}Cu_8Si_{16}$ (see Supplementary Note 1). The structure was optimized by comparing all formation energies of the possible positions of Si and Cu to take the disordered Si and Cu arrangements into account. For electronic structure calculations of $La_{12}Cu_8Si_{16}$, a cut-off energy of 400 eV and 7×4×6 of Monkhorst-Pack k-point meshes were used. To simulate hydrogen adsorption on the $LaCu_{0.67}Si_{1.33}$ surface, a $LaCu_{0.67}Si_{1.33}$ (11-22) surface was adopted, which was calculated to be the most stable surface among the low-index surfaces. The surface models were constructed as slab models including sufficient vacuum regions. 20 Å of vacuum width was used in the slab models to avoid artificial interactions between each slabs arrayed periodically. To avoid polar models, surface models in which each layer has the composition of $La_3Cu_2Si_4$ were adopted for the surface energy calculations. For the (11-22) surface, a 6×1 supercell on the a/b plane (4 layers along the c-direction) was used. For the $La_{24}Cu_{16}Si_{32}$ models, a cut-off energy of 400 eV and 9×2×1 of Monkhorst-Pack k-point meshes were used. The convergence criteria for energy and force were respectively $1.0×10^{-6}$ eV and $1.0×10^{-2}$ eV $Å^{-1}$ for all models. Atomic charges of La, Cu and Si were estimated with the Bader analysis of the charge density distributions.[20]

FT-IR measurements. Diffuse reflectance infrared Fourier transform (DRIFT) spectra were measured using a spectrometer (FT/IR-6100, Jasco) equipped with a mercury–cadmium–tellurium detector at a resolution of 4 cm^{-1}. An alumina sample cup containing approximately 30 mg of catalyst was introduced into a water-cooled stainless steel heat chamber equipped with KBr windows (STJ-0123-HP-LTV, S.T. Japan). The sample was heated at 200 °C under vacuum for 2 h and then cooled to room temperature. After the pretreatment, nitrobenzene, styrene, and nitrostyrene were supplied into the

system. The infrared spectrum of the sample at room temperature prior to the adsorption of substrates was used as the background for the difference spectra obtained by subtracting the backgrounds from the spectra of samples with adsorbed substrate.

Isotope H_2-D_2 Exchange Reaction. Before the reaction, the catalyst was heated in an Ar flow (10 mL·min^{-1}) at 200 °C for 0.5 h, followed by cooling to the desired temperature under He flow. The H_2-D_2 exchange reaction was conducted in a fixed bed quartz reactor that was supplied with an extra pure (99.99995%) mixture of H_2:D_2:Ar = 1:1:3. Reaction products (H_2, HD and D_2) were analysed with an online mass spectrometer (ANELVA, Quadrupole Mass Spectrometer). Trace amounts of HD formed in the experimental setup without the catalyst and this was used to correct the product concentrations.
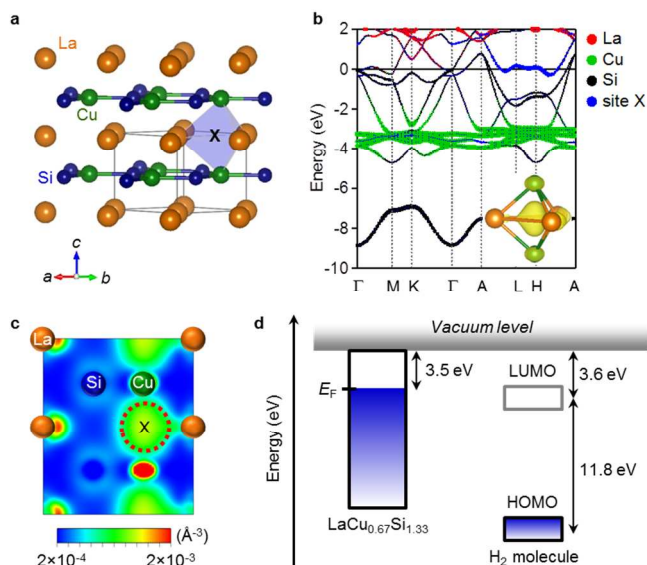
3. RESULTS AND DISCUSSION

Figure 1. Crystal and electronic structures of LaCuSi. a, Crystal structure of stoichiometric LaCuSi. The La, Cu and Si atoms are depicted as orange, green and blue balls, respectively. The La$_3$Cu$_2$ cage is emphasized using light-blue polyhedron. b, Calculated band structure of stoichiometric LaCuSi. The contribution of La, Cu, Si orbitals and vacant site X are highlighted using red, green, black and blue dots, respectively. The inset shows the free-electron density in the La$_3$Cu$_2$ cage with an isosurface of 0.0012 Å^{-3}. The contribution of site X in the band structure is emphasized using blue dots. c, Real space electronic density map for the (11-20) face calculated using the energy range of -0.05 < $E - E_F$ < 0.05 eV. d, Comparison of the Fermi level of LaCu$_{0.67}$Si$_{1.33}$ and the unoccupied (LUMO) state of H_2.

The crystal and electronic structures of stoichiometric LaCuSi were considered firstly (Figure 1a). LaCuSi crystallizes in a hexagonal structure and can be viewed as a metal-sandwiched variant of a honeycomb lattice. The Cu and Si atoms constitute a two-dimensional honeycomb network, whereas the La layers are located between each Cu/Si honeycomb layer with a distance of ca. 2.13 Å (ca. 4.25 Å for each Cu/Si honeycomb interlayer distance). This large interlayer distance leaves open interstitial spaces between the honeycomb layers, denoted as X, with fractional coordinates of (2/3, 1/3, 0). As in other hon-

eycomb lattice systems, Cu and Si sp orbitals are admixed and form three bonding σ and one π bands, whereas Cu 3d orbitals are located at ca. 4 eV below the Fermi level with a flat band feature (Figure 1b). Figures 1b and c show that LaCuSi has an interstitial band crossing the Fermi level, which coincides with the presence of the electron density peak at site X and is reminiscent of the previously reported AeAlSi (Ae = Ca, Sr, Ba) family of compounds and other electride materials, including C12A7:e$^-$ and Ca$_2$N.[21] These results imply that LaCuSi can be regarded as a intermetallic electride, which may realize improved electron donating ability. It is noted that the fundamental electronic structure remains essentially unchanged even in the disordered systems, i.e. the La$_3$Cu$_2$ cage still accommodates anionic electrons and gives rise to interstitial bands at the Fermi level (Figure S1).
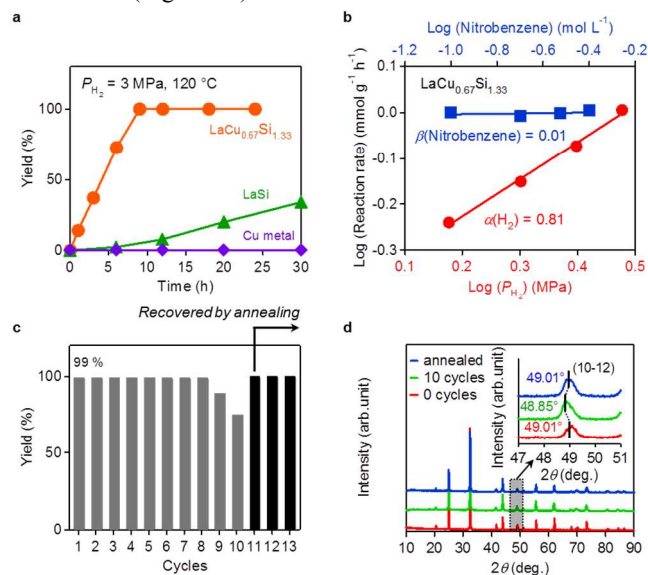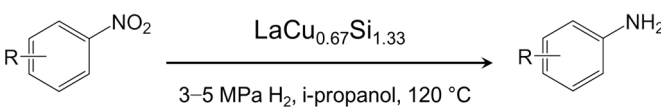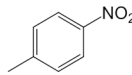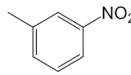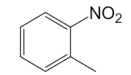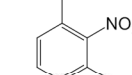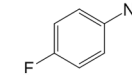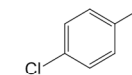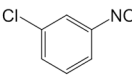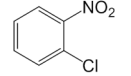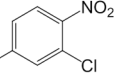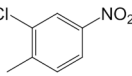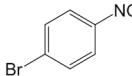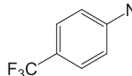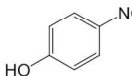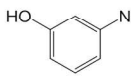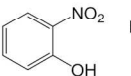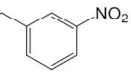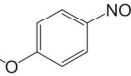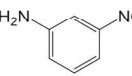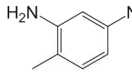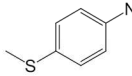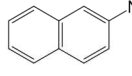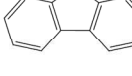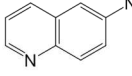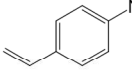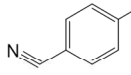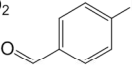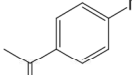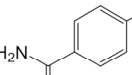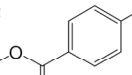

Figure 2. Kinetic studies and recycling of the nitrobenzene hydrogenation reaction. a, Time-dependent catalysis over LaCu$_{0.67}$Si$_{1.33}$ (S_{BET} = 0.95 m^2·g^{-1}), LaSi (S_{BET} = 0.85 m^2·g^{-1}), and elemental Cu (S_{BET} = 0.2 m^2·g^{-1}) catalysts. b, Dependence of reaction rate on nitrobenzene concentration and hydrogen pressure over the LaCu$_{0.67}$Si$_{1.33}$ catalyst. c, Recycling experiments over thirteen runs. After 10 runs, the LaCu$_{0.67}$Si$_{1.33}$ catalyst was recovered by annealing. Reaction conditions: 120 °C, 0.5 mmol nitrobenzene, 50 mg catalyst (Cu: 0.15 mmol), 3.0 MPa hydrogen, 5 mL i-propanol. d, Powder XRD patterns of as-prepared, used (after 10 cycles), and recovered LaCu$_{0.67}$Si$_{1.33}$ catalysts. The inset emphasizes the shift of the (10-12) peak for the corresponding samples.

As expected from density functional theory (DFT) calculations, LaCu$_{0.67}$Si$_{1.33}$ exhibits metallic conductivity with a carrier density of ca. 1×10^{22} cm^{-3}, which is 5 times higher than that of the well-studied LWF material C12A7:e$^-$ (Figure S2). The Pauli paramagnetism further confirmed the metallic nature of LaCu$_{0.67}$Si$_{1.33}$. The work function of LaCu$_{0.67}$Si$_{1.33}$, was measured to be $\Phi_{WF} \approx 3.5$ eV using photoelectron yield spectroscopy (PYS; Figure S3), which was much smaller than that for transition metals used for hydrogenation catalysts and was almost identical to that for metallic La (3.5 eV).[22] Given the LUMO of hydrogen molecules is located at 3.6 eV below the vacuum level,[23] the free electrons would be efficiently donated from LaCu$_{0.67}$Si$_{1.33}$ to the LUMOs of the starting components,

and expected to suppress the activation energy for H$_2$ dissocia-　　　tion (Figure 1d).

Table 1. LaCu$_{0.67}$Si$_{1.33}$-catalyzed hydrogenation of substituted nitroarenes.[a]

1: 99%, 12h　2: 99%, 12h　3: 99%, 12h　4: 99%, 18h　5: 99%, 27h　6: 99%, 72h

7: 99%, 72h　8: 99%, 72h　9: 97%, 84h　10: 99%, 84h　[b] 11: 99%, 48h　12: 99%, 54h

13: 98%, 84h　14: 97%, 84h　15: 99%, 92h　16: 96%, 97h　17: 99%, 24h　18: 99%, 30h

19: 99%, 30h　[b] 20: 93%, 280h　21: 96%, 96h　22: 97%, 72h　23: 99%, 39h

24: 95%, 48h　25: 96%, 60h　26: 98%, 36h　27: 93%, 48h　28: 87%, 60h　29: 99%, 192h

[a] Standard conditions: catalyst (50 mg), nitroarene (0.5 mmol), i-propanol (5 mL), 120 °C, H$_2$ (3 MPa). [b] H$_2$ (5 MPa). The yields given below the structure were determined using GC with n-hexadecane as an internal standard and GC-MS.

LaCu$_{0.67}$Si$_{1.33}$ has several unique properties among the hydrogenation catalysts. First, Cu atoms in LaCu$_{0.67}$Si$_{1.33}$ are distributed in the lattice framework and may serve as robust active sites even without metal loading. Second, the work function of LaCu$_{0.67}$Si$_{1.33}$ is 1.2 eV lower than elemental Cu and comparable to lanthanide elements, which should improve the electron donating ability of the Cu sites. The combination of both partially occupied Cu s-orbitals and the LWF encouraged us to attempt the hydrogenation of nitroarenes using LaCu$_{0.67}$Si$_{1.33}$ as a non-loaded catalyst. Preliminary hydrogenation experiments were conducted with nitrobenzene as a model substrate to evaluate the catalytic activity. In this reaction, i-propanol was determined to be the optimal solvent and the reaction temperature was set to 120 °C. While i-propanol can be generally used as a hydrogen donor reagent, it was confirmed that the reactive hydrogen source simply comes from the hydrogen molecules in this reaction (Table S1). As shown in Figure 2a, LaCu$_{0.67}$Si$_{1.33}$ hydrogenates nitrobenzene without producing any intermediates or by-products during the entire reaction process and the reaction rate reached 1.33 mmol·g^{-1}·h^{-1} under 3.0 MPa to yield 99% aniline in 9 h.

LaCu$_{0.67}$Si$_{1.33}$ can also catalyse the reaction even in a solvent-free system at a mass production (50 mmol) scale (Figure S4). LaCu$_{0.67}$Si$_{1.33}$ was confirmed to continually produced aniline and the reaction was completed in 60 h with a 99% yield under optimized conditions. The reaction rates are sensitive to the hydrogen pressure but independent of the nitrobenzene concentration, which results in kinetic reaction orders of α(H$_2$) = 0.81 and β(nitrobenzene) = 0.01, respectively (Figure 2b). These contrastive kinetic parameters imply that LaCu$_{0.67}$Si$_{1.33}$ breaks through the limitation of nitrobenzene activation, and hydrogen activation is the rate-controlling step. Note that the reaction proceeds only in the presence of LaCu$_{0.67}$Si$_{1.33}$, and no more aniline can be produced after removal of the catalyst during the reaction process (Figure S5). Moreover, an inductively coupled plasma analysis revealed that La, Cu and Si species in the filtrate were below the detection limit (0.007 ppm).

Elemental Cu ($\Phi_{WF} \approx 4.7$ eV) and LaSi ($\Phi_{WF} \approx 3.6$ eV) were also tested under the same reaction conditions as reference materials to evaluate the effect of electron donation and Cu sites. It is noted that strong electron donating ability and Cu

sites are absent in elemental Cu and LaSi, respectively.[24] Both of them exhibit poorer catalytic activity for the hydrogenation reaction, which suggests that the Cu atoms involved in LWF materials serve as effective active sites, which will be discussed further with respect to DFT calculations. Given the catalyst hosts 0.67 Cu atoms per surface area of 47.4 $Å^2$ in a single unit cell of $LaCu_{0.67}Si_{1.33}$, the turnover frequency (TOF) could be estimated to be 3769 h^{-1} for conventional (Figure 2a) and 5084 h^{-1} for mass production reaction conditions (Figure S4), respectively. Such TOF values are an order of magnitude higher than those reported for current ubiquitous metal-based heterogeneous catalysts (Table S2).[25] Furthermore, $LaCu_{0.67}Si_{1.33}$ is superior to those catalytic systems with easily reducible groups (Table S3).[25,26]

$LaCu_{0.67}Si_{1.33}$ has excellent chemical stability and recyclability. The catalytic activity of $LaCu_{0.67}Si_{1.33}$ is stable over eight cycles (stability test at low conversion level is also shown in Figure S6), and decompositions of the catalyst, such as by the condensation of Cu atoms, was not identified from powder X-ray diffraction (XRD) measurements after the reactions were completed (Figure 2c and 2d). Instead, the unit cell was observed to be slightly expanded, plausibly due to hydrogen incorporation (Figure S7). Temperature programmed desorption (TPD) measurements confirmed that the used catalyst (after 10 reaction cycles) contains ca. 0.21 hydrogens per formula unit, which desorb above ca. 420 °C (Figure S8). The catalytic activity starts to degrade with an increase in the hydrogen content and ca. 30% of the conversion ratio was lost in the tenth run. We argue that the degraded activity could be attributed to the incorporated hydrogen, which captures free electrons and lowers the electron donating ability as with other LWF materials such as $C12A7:e^-$.[8] However it should be noted that the rate of hydrogen incorporated into the $LaCu_{0.67}Si_{1.33}$ was quite slow, which can be confirmed from the absence of both adsorption and desorption of H_2 in a H_2-TPR measurement (Figure S9). The catalytic activity was therefore recovered after removal of the hydrogen from $LaCu_{0.67}Si_{1.33}H_{0.21}$ by annealing the used catalyst at 550 °C for 2 h under an Ar flow. After the heating process, the expanded unit cell volume returned to the original value and the resulting $LaCu_{0.67}Si_{1.33}$ could be reused without loss in activity for at least three subsequent runs (Figure 2c and 2d).

Various nitroarenes were tested under the optimized reaction conditions to examine the general applicability of the $LaCu_{0.67}Si_{1.33}$ catalyst for hydrogenation reactions. The results summarized in Table 1 indicate that good yields (>93%) of the desired products could be obtained for all the substrates. Notably, the $LaCu_{0.67}Si_{1.33}$ catalyst also exhibited high chemoselectivity towards the nitro group in the presence of some very easily reducible moieties, which highlight the good tolerance of the various functional groups with this $LaCu_{0.67}Si_{1.33}$ based catalytic system towards the selective hydrogenation of nitroarenes.

The kinetic isotope effect has been firstly considered in the hydrogenation of nitrobenzene under H_2 and D_2 at 120 °C over $LaCu_{0.67}Si_{1.33}$. The reaction rates under H_2 and D_2 were estimated to be r_H = 1.33 mmol·g^{-1}·h^{-1} and r_D = 0.35 mmol·g^{-1}·h^{-1}, respectively (Figure S10). These results indicate the kinetic isotope effect to be r_H/r_D = 3.8 (>1) due to the differences between the bond dissociation energy of H_2 and D_2, implying that the cleavage of hydrogen molecules would be the rate-determining step in the reaction, which is consistent with the

kinetic analysis, as shown in the Figure 2b. Hydrogen activation is the key step in this reaction; therefore, the hydrogen adsorption process on the surface of $LaCu_{0.67}Si_{1.33}$ was examined using DFT calculations. Here, the (11-22) surface of $LaCu_{0.67}Si_{1.33}$ was calculated to be the most stable exposed face. As shown in Figure S11, regardless of the initial site of the dissociated hydrogen atom located on La or Cu sites, the hydrogen atoms tend to be automatically relaxed onto the Cu side with an adsorption energy of −0.95 eV. The length of the Cu−H bond was estimated to be 1.64 Å, which is similar to the intrinsic length 1.57 Å of CuH.[27] This indicates a clear contrast of H adsorption on Cu(111); the most stable adsorption site of H on Cu(111) is the threefold hollow site, and the calculated adsorption energy is −0.22 eV, which indicates a much stronger adsorption of H on the Cu site of $LaCu_{0.67}Si_{1.33}$ than on the Cu(111) face. However, the length of La-H was extended to 2.46 Å, compared with the intrinsic length 2.0 Å of LaH,[28] which suggests that the formation of the stabilized active H species is favored at the Cu sites. Moreover, the calculated adsorption energy of −0.28 eV for a hydrogen atom on a Si site is 3 times smaller than that on a Cu site (Figure S12), which indicates more stable adsorption for the hydrogen atom on Cu sites than on Si sites. The present DFT calculations provided the most stable adsorption configuration for hydrogen atoms on the (11-22) surface of $LaCu_{0.67}Si_{1.33}$ through the Cu sites, which demonstrates that the Cu species is the active site for hydrogen dissociation.

Through the further DFT calculation on H_2 dissociation, we proposed two possible routes for the cleavage of H_2 on $LaCu_{0.67}Si_{1.33}$ (Figure S13). H_2 dissociation occurs preferentially on the Cu-Cu site with a relative larger adsorption energy of -1.22 eV than those on other sites, which results in the formation of both negative charged H (ca. -0.5e) via homolytic cleavage of H_2. Another possible site for H_2 dissociation is the Cu-Si site with a bit smaller adsorption energy of -1.18 eV. The calculated charge density of adsorbed H on Cu and Si is -0.51 e and -1.19 e respectively, indicating the homolytic manner of H_2 cleavage with a charge deviation. Although the detailed mechanism remains not decisive at this stage, it is important to emphasize that electron transfer from the negative charged Cu to H_2 could be the key factor for H_2 dissociation and the involved Cu sites in $LaCu_{0.67}Si_{1.33}$ should be the active sites for H_2 activation.
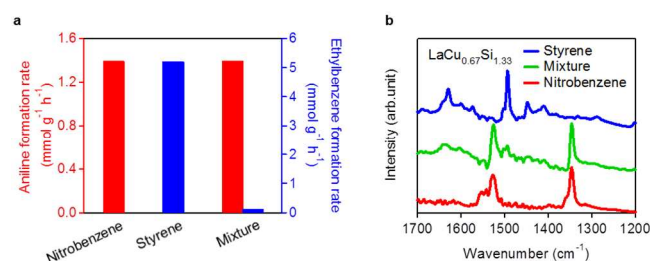
Figure 3. Catalytic selectivity and FT-IR spectra of $LaCu_{0.67}Si_{1.33}$. a, Competitive reaction over $LaCu_{0.67}Si_{1.33}$ catalyst. Styrene, nitrobenzene and a mixture of both were used as substrates over $LaCu_{0.67}Si_{1.33}$ catalyst. Reaction conditions: 120 °C, 3.0 MPa hydrogen, 50 mg catalyst, 5 mL *i*-propanol. Substrates: 0.5 mmol nitrobenzene or styrene; competitive reaction: 0.25 mmol nitrobenzene and 0.25 mmol styrene. b, DRIFT spectra of adsorption of nitrobenzene, styrene, and a mixture of nitrobenzene and styrene with a 1:1 molar ratio on $LaCu_{0.67}Si_{1.33}$ at 25 °C.

For the hydrogenation reaction of nitroarenes to corresponding amines, two routes (monomeric route and dimeric route in Figure S14) have been proposed.[29] The fact that the conversion of azoxybenzene (Figure S15) was much slower than that of nitrobenzene under fixed experimental conditions excludes the possibility of dimeric route in this $LaCu_{0.67}Si_{1.33}$ catalytic system. As we know, the adsorption of nitroarene via the oxygen atoms in nitro group on the catalyst surface is a key step for the selective hydrogenation of nitro group.[30] Therefore, adsorption of oxygen on the surface of $LaCu_{0.67}Si_{1.33}$ was examined by DFT calculations to understand the origin of the interaction between catalyst surface and reactants.[31] The calculated adsorption energy of O over the $LaCu_{0.67}Si_{1.33}$(11-22) is −4.63 eV, larger than that on Cu(111) −1.50 eV, indicating the much stronger interaction of reactants molecules on $LaCu_{0.67}Si_{1.33}$ surface (Figure S16, S17). It should be noted that $LaCu_{0.67}Si_{1.33}$ is air-stable and has high resistance to water regardless of high oxygen affinity (Figure S18). Moreover, the most stable adsorption site of O on $LaCu_{0.67}Si_{1.33}$ is the hollow site composed of one Cu and two La atoms (h_LLC) (Figure S16). It can be considered that nitrobenzene molecule preferentially binds with the h_LLC site via oxygen atoms of nitro group. In addition, hydrogen activation also occurs on the Cu site (Figure S11, S13). Accordingly, the preferential adsorption of nitro group at h_LLC site and hydrogen activation on Cu site give rise to the good selectivity for the formation of desired product.
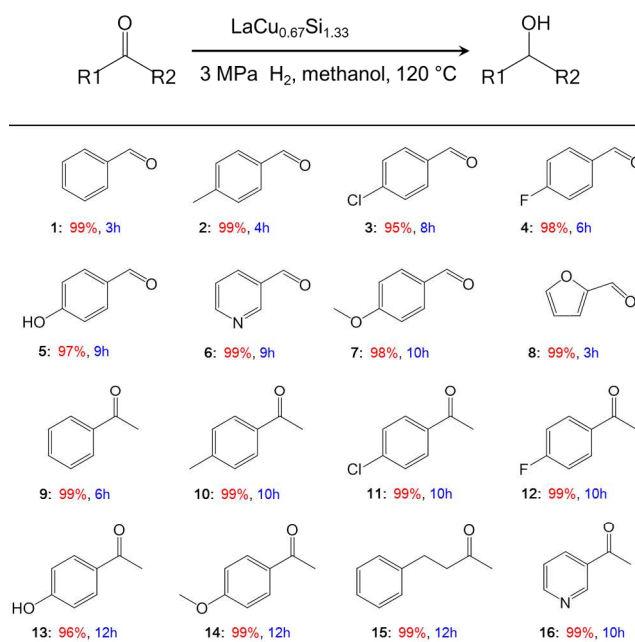
It is noteworthy that the $LaCu_{0.67}Si_{1.33}$ catalyst selectively hydrogenated the nitro group of the 4-nitrostyrene (entry 24 of the Table 1), in which the vinyl group is easily hydrogenated. To elucidate the underlying factors that afford the selective hydrogenation of nitroarenes, kinetic experiments and Fourier transform-infrared (FT-IR) spectroscopy measurements were performed on the $LaCu_{0.67}Si_{1.33}$ catalyst with styrene and nitrobenzene as substrates. The reaction rate for the sole hydrogenation of styrene and nitrobenzene were 5.19 and 1.33 mmol·g^{-1}h^{-1} under the same reaction conditions, respectively. This result indicates that the intrinsic activity for the reduction of olefinic group on $LaCu_{0.67}Si_{1.33}$ is much larger than that of the nitro group. However, for the styrene/nitrobenzene mixed substrate, the reaction rate of styrene was significantly suppressed, whereas nitrobenzene was selectively hydrogenated (Figure 3a). This observed selectivity can be attributed to the strong interaction between the nitro group and $LaCu_{0.67}Si_{1.33}$ catalyst. As shown in Figure 3b, the IR vibrational bands of nitro groups ($v_{as}(NO_2)$: 1526 cm^{-1} and $v_s(NO_2)$: 1350 cm^{-1}) and vinyl groups ($v(C=C)$: 1630 cm^{-1} and $\delta(=C-H)$: 1411 cm^{-1}) can be observed on the $LaCu_{0.67}Si_{1.33}$ catalyst when only styrene or nitrobenzene were used (see Figure 3b).[32] However, if the nitrobenzene/styrene mixture was used as a substrate, then the IR absorption peaks corresponding to the vinyl groups were suppressed and the spectrum became almost identical to that for the sole nitrobenzene case (Figure 3b). Although the broad peaks due to the vinyl groups of styrene were also observed in the mixture, the intensity was much lower than that of nitro groups, implying the preferential adsorption of nitro groups on the catalyst surface. These results are consistent with the kinetic experiments, in which the reaction rate obtained with styrene was suppressed with the styrene/nitrobenzene mixture. Consequently, the preferential adsorption of nitro groups onto the surface of $LaCu_{0.67}Si_{1.33}$

with high oxygen affinity (shown in Figure S16) accounts for the excellent selectivity.

Furthermore, the high oxygen affinity of $LaCu_{0.67}Si_{1.33}$ contributes to selective hydrogenation of nitro group in the presence of carbonyl group (entries 26-29, Table 1). One possible explanation for the selective hydrogenation of nitro group is that the adsorption of nitro group to the $LaCu_{0.67}Si_{1.33}$ surface occurs at the most stable adsorption configuration. It can be considered that nitroarene is adsorbed on the catalyst surface via two oxygen atoms in nitro group, whereas carbonyl compounds interact with the catalyst via one oxygen atom of C=O bond. Hence, we can deduce that the interaction between the catalyst and nitroarene is much stronger than the case of carbonyl compounds, leading to high selective hydrogenation of nitro group. This hypothesis is supported by the following results. Nitrobenzene hydrogenation took place preferentially over $LaCu_{0.67}Si_{1.33}$ (Figure S19a) when a mixture of nitrobenzene and benzaldehyde was used as substrate. The reaction rate in the mixture system is almost identical to that of hydrogenation of pure nitrobenzene. However, the reductive coupling of aniline and benzaldehyde occurred immediately once aniline formed from the hydrogenation of nitrobenzene. As a result, benzylideneaniline and phenylbenzylamine were mainly formed as products (Figure S19b) and a trace amount of aniline and trace benzyl alcohol were also detected. In the case of coexistence of nitro group and carbonyl in entry 26 and 27, the presence of electron-withdrawing substituent led to less reactive anilines.[33] So the reaction exhibit high selectivity to aniline product. Thus, the present results demonstrate that the interaction between $LaCu_{0.67}Si_{1.33}$ and nitro group is much stronger than that of carbonyl group, which results in the chemoselective hydrogenation of nitro group.

Table 2. $LaCu_{0.67}Si_{1.33}$-catalyzed hydrogenation of different aldehydes and ketones.[a]

1: 99%, 3h 2: 99%, 4h 3: 95%, 8h 4: 98%, 6h

5: 97%, 9h 6: 99%, 9h 7: 98%, 10h 8: 99%, 3h

9: 99%, 6h 10: 99%, 10h 11: 99%, 10h 12: 99%, 10h

13: 96%, 12h 14: 99%, 12h 15: 99%, 12h 16: 99%, 10h

[a] Standard conditions: catalyst (50 mg), aldehyde/ketone (0.5 mmol), methanol (5 mL), 120 °C, H$_2$ (3 MPa). The yields given below the structure were determined using GC and GC-MS.

Due to high oxygen affinity of $LaCu_{0.67}Si_{1.33}$, we became interested in testing this $LaCu_{0.67}Si_{1.33}$ catalyst for the hydrogenation of other oxygen-containing functional group such as aldehydes and ketones. As shown in Figure S20, both benzaldehyde and acetophenone were hydrogenated into the corresponding alcohols over $LaCu_{0.67}Si_{1.33}$ catalyst in 3 h and 6 h without any additives or promoters. The calculated TOF values of 18250 h^{-1} and 4874 h^{-1} for benzaldehyde and acetophenone hydrogenation were greater than those of reported transition metal based catalysts.[34] Kinetic study of these hydrogenation reactions revealed that $LaCu_{0.67}Si_{1.33}$ catalyst has a first order relationship with respect to H_2 pressure and a zero order dependence on each substrate. These results suggest that the cleavage of the H–H bond is the rate-determining step, which is consistent with the results of nitrobenzene hydrogenation. The $LaCu_{0.67}Si_{1.33}$ catalyst also exhibits high chemoselectivity for various benzaldehydes or acetophenones bearing different functional groups (Table 2).

The H_2−D_2 exchange reaction was investigated to further clarify the origin of the superior hydrogenation activity of $LaCu_{0.67}Si_{1.33}$. As shown in Figure 4a, $LaCu_{0.67}Si_{1.33}$ exhibits a much higher rate of HD formation than LaSi and elemental Cu, although these catalysts have similar surface areas. The lower activity over the LaSi sample is mainly attributed to the absence of Cu sites in the LaSi matrix. This result strongly suggests that Cu sites in $LaCu_{0.67}Si_{1.33}$ function as active sites for hydrogen dissociation. Meanwhile, the Bader charge analysis shows that the Cu sites on (11-22) surface of $LaCu_{0.67}Si_{1.33}$ are negatively charged ($−0.5|e| \sim −0.6|e|$), while the La sites are positively charged ($+1.3|e| \sim +1.4|e|$), as shown in Figure S21. Therefore, the electron transfer from La to Cu increases the electron density of Cu, which reduces the energy barrier for H_2 dissociation.[35] It should be noted that the activation energy for the H_2-D_2 exchange reaction on $LaCu_{0.67}Si_{1.33}$ ($E_a = 14.8$ kJ·mol^{-1}) is much lower than previously studied noble metal catalyst, such as Au ($E_a = 36.2$ kJ·mol^{-1}) and Ag ($E_a = 45.2$ kJ·mol^{-1}) under the similar reaction conditions.[36] However, it is well known that the rate of hydrogen adsorption over pure Cu metal is very low due to its high energy barrier for H_2 dissociation (ca. 58 kJ·mol^{-1}).[37] Our experimental results confirmed that Cu metal exhibits low catalytic activity due to higher activation energy (64.1 kJ·mol^{-1}) for the H_2−D_2 exchange reaction (Figure 4b). On the other hand, the activation energy is significantly lowered over the $LaCu_{0.67}Si_{1.33}$ catalyst, which clearly demonstrates that hydrogen dissociation over the Cu sites is promoted by the high electron donating characteristic of $LaCu_{0.67}Si_{1.33}$ with a LWF ($\Phi_{WF} \approx 3.5$ eV). Meanwhile, the rate constant of HD formation over $LaCu_{0.67}Si_{1.33}$ was also much higher than that of bare Cu metal (Figure S22, Table S4). Generally, metal-H_2 binding is governed by both σ-donation from H_2 to metal and π-back-donation from metal to H_2, and the cleavage of H-H bond is effectively enhanced by the π-back-donation if the electron transfer from metal to H_2 is significantly large. This fact is well recognized in the metal-hydride complex system.[38] Hence, our experimental result can be a clear evidence for the electron transfer from $LaCu_{0.67}Si_{1.33}$ electride to H_2 molecule. This result also implies that the hydrogen activation ability of Cu is enhanced when Cu is located in the framework of a LWF material. Based on the specific surface area of the $LaCu_{0.67}Si_{1.33}$ (0.95 m^2 g^{-1}) and Cu (0.2 m^2 g^{-1}) samples, the number of surface Cu sites on $LaCu_{0.67}Si_{1.33}$ (0.37 μmol g^{-1}) is one order of magnitude lower than that on

Cu (6.0 μmol g^{-1}). Accordingly, the activity of $LaCu_{0.67}Si_{1.33}$ is much superior to that of Cu. These observations clearly demonstrate that the activation of the chemisorbed hydrogen molecule plays a crucial role in the net catalytic performance. This hypothesis is commonly accepted for catalytic reactions over transition metal complex catalysts, i.e., electron transfer from ligands to the transition metals (due to partially occupied *s* and *d*-orbitals) plays an important role in catalytic performance.[39]
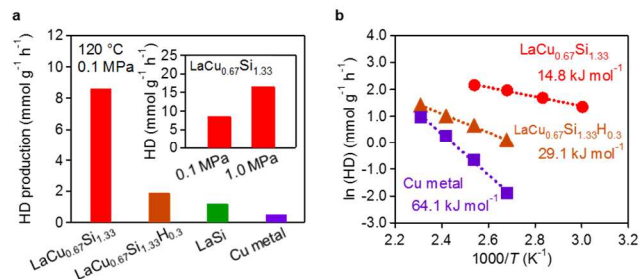

Figure 4. Isotope H_2−D_2 Exchange Reaction. a, Rate for HD formation over $LaCu_{0.67}Si_{1.33}$, $LaCu_{0.67}Si_{1.33}H_{0.3}$, LaSi and Cu catalysts under 0.1 MPa at 120 °C. The inset represents the rate for HD formation over $LaCu_{0.67}Si_{1.33}$ under 0.1 MPa and 1.0 MPa of H_2/D_2 pressure. b, Arrhenius plots for $LaCu_{0.67}Si_{1.33}$ and $LaCu_{0.67}Si_{1.33}H_{0.3}$ catalysts. Apparent activation energy calculated from Arrhenius plots for the reaction rate in the temperature range of 60–160 °C.

To further investigate the effect of the electron donating ability, the corresponding H^- incorporated sample ($LaCu_{0.67}Si_{1.33}H_{0.3}$), in which anionic electron is captured by hydrogen to form H^-, was prepared by the heat treatment of $LaCu_{0.67}Si_{1.33}$ under H_2 gas flow for 24 h (Figure S23, S24) and the catalytic reaction under identical conditions was also tested for comparison. As expected, the $LaCu_{0.67}Si_{1.33}H_{0.3}$ sample exhibited a lower HD production rate (1.8 mmol·g^{-1} h^{-1}) and a larger activation energy than hydrogen-free $LaCu_{0.67}Si_{1.33}$ (Figure S25), which led to a lower reaction rate for the hydrogenation of nitrobenzene (Figure S26). FT-IR results revealed that the adsorption behavior of the $LaCu_{0.67}Si_{1.33}$ and $LaCu_{0.67}Si_{1.33}H_{0.3}$ samples is not significantly different (Figure S27). Therefore, it can be concluded that the hydrogenation of nitroarene over $LaCu_{0.67}Si_{1.33}H_{0.3}$ is largely limited by the rate of H_2 dissociation due to the large activation barrier to dissociate H_2. The same phenomenon was observed in the repeated reaction (Figure 2c); i.e., $LaCu_{0.67}Si_{1.33}$ is deactivated by the incorporation of hydrogen into the lattice during repeated reaction, but the activity is totally recovered when hydrogen is removed from $LaCu_{0.67}Si_{1.33}H_{0.3}$ by annealing. The presence of anionic electrons in $LaCu_{0.67}Si_{1.33}$ plays a crucial role in the activation of H_2 molecules and the catalytic activity for the selective hydrogenation of nitroarenes. Corma *et al.* inferred by the Hougen–Watson/Langmuir–Hinshelwood kinetic model that catalysts that activate H_2 fastest were the most active for the hydrogenation of nitro compounds.[40] Our results are well explained by the kinetic model inferred.

4. CONCLUSIONS

In summary, the Cu-based intermetallic electride $LaCu_{0.67}Si_{1.33}$ was found to exhibit excellent catalytic activity for various selective hydrogenation reactions. $LaCu_{0.67}Si_{1.33}$ possesses both a high carrier density and a LWF, and exhibits much

higher activity than conventional transition metal nanoparticles on oxide or carbon supports. Mechanistic studies demonstrated that electron transfer from anionic electrons in $LaCu_{0.67}Si_{1.33}$ bulk promotes H_2 dissociation on the highly charged anti-bonding orbital of molecular hydrogen, which is the rate-determining step of the investigated hydrogenation reactions. The preferential adsorption of the reactant on the catalyst surface through the oxygen-containing group leads to excellent selectivity. $LaCu_{0.67}Si_{1.33}$ itself serves as a hydrogenation catalyst without the need for metal loading on the surface; therefore, this study establishes transition metal based LWF materials as new catalysts for such reactions, which should simplify the entire preparation and reaction processes for hydrogenation.

Supporting Information

The Supporting Information is available free of charge on the ACS Publications website. brief description (file type, i.e., PDF) brief description (file type, i.e., PDF)

AUTHOR INFORMATION

Corresponding Author

e-mail: hosono@msl.titech.ac.jp

Author Contributions

[†]These authors contributed equally.

Notes

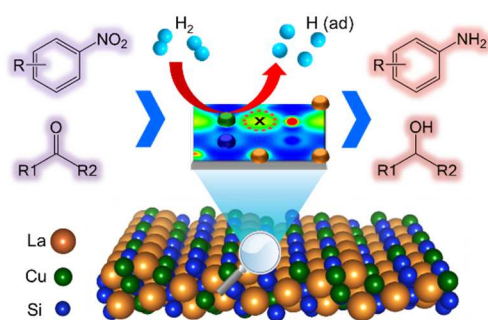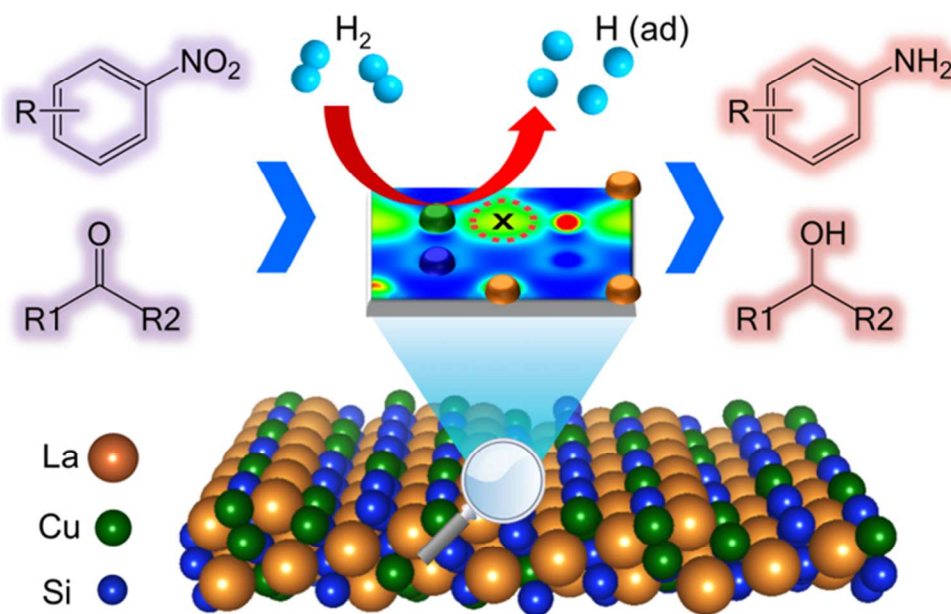The authors declare no competing financial interests.

ACKNOWLEDGMENT

REFERENCES

(1). (a) Corma, A.; Serna, P. *Science* **2006**, *313*, 332; (b) Jagadeesh, R. V.; Surkus, A. E.; Junge, H.; Pohl, M.-M.; Radnik, J.; Rabeah, J.; Huan, H.; Schünemann, V.; Brückner, A.; Beller, M. *Science* **2013**, *342*, 1073.

(2). (a) Zambelli, T.; Wintterlin, J.; Trost, J.; Ertl, G. *Science* **1996**, *273*, 1688; (b) Farmer, J. A.; Campbell, C. T. *Science* **2010**, *329*, 933; (c) Li, X. H.; Wang, X.; Antonietti, M. *Chem. Sci.* **2012**, *3*, 2170.

(3). (a) Liu, P.; Zhao, Y.; Qin, R.; Mo, S.; Chen, G.; Gu, L.; Chevrier, D. M.; Zhang, P.; Guo, Q.; Zang, D.; Wu, B.; Fu, G.; Zheng, N. *Science* **2016**, *352*, 797; (b) Qiao, B.; Wang, A.; Yang, X.; Allard, L. F.; Jiang, Z.; Cui, Y.; Liu, J.; Li, J.; Zhang, T. *Nat. Chem.* **2011**, *3*, 634; (c) Moliner, M.; Gabay, J. E.; Kliewer, C. E.; Carr, R. T.; Guzman, J.; Casty, G. L.; Serna, P.; Corma, A. *J. Am. Chem. Soc.* **2016**, *138*, 15743; (d) Ge, J.; He, D.; Chen, W.; Ju, H.; Zhang, H.; Chao, T., Wang, X.; You, R.; Lin, Y.; Wang, Y.; Zhu, J.; Li, H.; Xiao, B.; Huang, W.; Wu, Y.; Hong, X.; Li, Y. *J. Am. Chem. Soc.* **2016**, *138*, 13850; (e) Vilé, G.; Albani, D.; Nachtegaal, M.; Chen, Z.; Dontsova, D.; Antonietti, M.; López, N.; Pérez-Ramírez, J. *Angew. Chem. Int. Ed.* **2015**, *54*, 11265.

(4). (a) Jones, J.; Xiong, H.; DeLaRiva, A. T.; Peterson, E. J.; Pham, H.; Challa, S. R.; Qi, G.; Oh, S.; Wiebenga, M. H.; Hernández, X. I. P.; Wang, Y.; Datye, A. K. *Science* **2016**, *353*, 150; (b) Liu, L.; Díaz, U.; Arenal, R.; Agostini, G.; Concepción, P.; Corma, A. *Nat. Mater.* **2017**, *16*, 132; (c) Yan, H.; Cheng, H.; Yi, H.; Lin, Y.; Yao, T.; Wang, C.; Li, J.; Wei, S.; Lu, J. *J. Am. Chem. Soc.* **2015**, *137*, 10484.

(5). (a) Dye, J. L. *Science* **1990**, *247*, 663; (b) Dye, J. L. *Science* **2003**, *301*, 607.

(6). (a) Toda, Y.; Hirayama, H.; Kuganathan, N.; Torrisi, A.; Sushko, P. V.; Hosono, H. *Nat. Commun.* **2013**, *4*, 2378; (b) Choi, S.; Kim, Y. J.; Kim, S. M.; Yang, J. W.; Kim, S. W.; Cho, E. J. *Nat. Commun.* **2014**, *5*, 4881; (c) Kim, S. M.; Yoo, H. S.; Hosono, H.; Yang, J. W.; Kim, S. W. *Sci. Rep.* **2015**, *5*, 10366.

(7). (a) Kitano, M.; Kanbara, S.; Inoue, Y.; Kuganathan, N.; Sushko, P. V.; Yokoyama, T.; Hara, M.; Hosono, H. *Nat. Commun.* **2015**, *6*, 6731; (b) Kanbara, S.; Kitano, M.; Inoue, Y.; Yokoyama, T.; Hara, M.; Hosono, H. *J. Am. Chem. Soc.* **2015**, *137*, 14517; (c) Ye. T. N.; Li, J.; Kitano, M.; Sasase, M.; Hosono, H. *Chem. Sci.* **2016**, *7*, 5969; (d) Ye. T. N.; Li, J.; Kitano, M.; Hosono, H. *Green. Chem.* **2017**, *19*, 749.

(8). Kitano, M.; Inoue, Y.; Yamazaki, Y.; Hayashi, F.; Kanbara, S.; Matsuishi, S.; Yokoyama, T.; Kim, S.; Hara, M.; Hosono, H. *Nat. Chem.* **2012**, *4*, 934.

(9). Matsuishi, S. Toda, Y.; Miyakawa, M.; Hayashi, K.; Kamiya, T.; Hirano, M.; Tanaka, I.; Hosono, H. *Science* **2003**, *301*, 626.

(10). Kuganathan, N., Hosono, H., Shluger, A. L.; Sushko, P. V. *J. Am. Chem. Soc.* **2014**, *136*, 2216.

(11). (a) Lu, Y. F.; Li, J.; Tada, T.; Toda, Y. Ueda, S.; Yokoyama, T.; Kitano, M.; Hosono, H. *J. Am. Chem. Soc.* **2016**, *138*, 3970; (b) Kitano, M.; Inoue, Y.; Ishikawa, H.; Yamagata, K.; Nakao, T.; Tada, T.; Matsuishi, S.; Yokoyama, T.; Hara, M.; Hosono, H. *Chem. Sci.* **2016**, *7*, 4036.

(12). (a) Studt, F.; Abild-Pedersen, F.; Bligaard, T.; Sørensen, R. Z.; Christensen, C. H.; Nørskov, J. K. *Science* **2008**, *320*, 1320; (b) Armbrüster, M.; Kovnir, K.; Friedrich, M.; Teschner, D.; Wowsnick, G.; Hahne, M.; Gille, P.; Szentmiklósi, L.; Feuerbacher, M.; Heggen, M.; Girgsdies, F.; Rosenthal, D.; Schlögl, R.; Grin, Y. *Nat. Mater.* **2012**, *11*, 690.

(13). (a) Armbrüster, M.; Kovnir, K.; Behrens, M.; Teschner, D.; Grin, Y.; Schlögl, R. *J. Am. Chem. Soc.* **2010**, *132*, 14745; (b) Furukawa. S.; Komatsu, T. *ACS Catal.* **2017**, *7*, 735.

(14). (a) Armbrüster, M.; Wowsnick, G.; Friedrich, M.; Heggen, M.; Cardoso-Gil, R. *J. Am. Chem. Soc.* **2011**, *133*, 9112; (b) Feng, Q.; Zhao, S.; Wang, Y.; Dong, J.; Chen, W.; He, D.; Wang, D.; Yang, J.; Zhu, Y.; Zhu, H.; Gu, L.; Li, Z.; Liu, Y.; Yu, R.; Li, J.; Li, Y. *J. Am. Chem. Soc.* **2017**, *139*, 7294; (c) Liu, Y.; Liu, X.; Feng, Q.; He, D.; Zhang, L.; Lian, C.; Shen, R.; Zhao, G.; Ji, Y.; Wang, D.; Zhou, G.; Li, Y. *Adv. Mater.* **2016**, *28*, 4747.

(15). Gupta, S.; Suresh, K. G. *J. Alloys Compd.* **2015**, *618*, 562.

(16). (a) Kresse, G.; Furthmüller, J. *Comput. Mater. Sci.* **1996**, *6*, 15; (b) Kresse, G.; Furthmüller, J. *Phys. Rev. B* **1996**, *54*, 11169.

(17). Perdew, J. P.; Burke, K.; Ernzerhof, M. *Phys. Rev. Lett.* **1996**, *77*, 3865.

(18). (a) Blöchl, P. E. *Phys. Rev. B* **1994**, *50*, 17953; (b) Kresse, G.; Joubert, D. *Phys. Rev. B* **1999**, *50*, 1758.

(19). Monkhorst, H. J.; Pack, J. D. *Phys. Rev. B: Condens. Matter* **1976**, *13*, 5188.

(20). Tang, W.; Sanville, E.; Henkelman, G. *J. Phys. Condens. Matter.* **2009**, *21*, 084204.

(21). (a) Lu, Y. F.; Tada, T.; Toda, Y. Ueda, S.; Wu, J.; Li, J.; Horiba, K.; Kumigashira, H.; Zhang, Y.; Hosono, H. *Phys. Rev. B* **2017**, *95*, 125117; (b) Lee, K.; Kim, S. W.; Toda, Y.; Matsuishi, S.; Hosono, H. *Nature* **2013**, *494*, 336.

(22). Michaelson, H. B. *J. Appl. Phys.* **1977**, *48*, 4729.

(23). Zhang, G.; Musgrave, C. B. *J. Phys. Chem. A*, **2007**, *111*, 1554.

(24). (a) Gartland, P. O.; Berge, S. B.; Slagsvold, J. *Phys. Rev. Lett.* **1972**, *28*, 738; (b) Drummond, T. J. *SciTech Connect,* **1999**, Available at https://www.osti.gov/scitech/biblio/3597.

(25). (a) Jagadeesh, R. V.; Surkus, A. E.; Junge, H.; Pohl, M.-M.; Radnik, J.; Rabeah, J.; Huan, H.; Schünemann, V.; Brückner,

A.; Beller, M. *Science* **2013**, *342*, 1073; (b) Westerhaus, F. A.; Jagadeesh, R. V.; Wienhöfer, G.; Pohl, M.-M.; Radnik, J.; Surkus, A.-E.; Rabeah, J.; Junge, K.; Junge, H.; Nielsen, M.; Brückner, A.; Beller, M. *Nat. Chem.* **2013**, *5*, 537; (c) Schwob, T.; Kempe, R. *Angew. Chem. Int. Ed.* **2016**, *55*, 15175; (d) Wei, Z.; Wang, J.; Mao, S.; Su, D.; Jin, H.; Wang, Y.; Xu, F.; Li, H.; Wang, Y. *ACS Catal.* **2015**, *5*, 4783.

(26). (a) Liu, L.; Concepción, P.; Corma, A. *J. Catal.* **2016**, *340*, 1; (b) Ren, Y.; Wei, H.; Yin, G.; Zhang, L.; Wang, A.; Zhang, T. *Chem. Commun.* **2017**, *53*, 1969; (c) Hahn, G.; Ewert, J.; Denner, C.; Tilgner, D.; Kempe, R. *ChemCatChem.* **2016**, *8*, 2461.

(27). Calvi, R. M. D.; Andrews, D. H.; Lineberger, W. C. *Chem. Phys. Lett.* **2007**, *442*, 12.

(28). Hong, G.; Dolg, M.; Li, L. *Chem. Phys. Lett.* **2001**, *334*, 396.

(29). Ji, P.; Manna, K.; Lin, Z.; Feng, X.; Urban, A.; Song, Y.; Lin, W. *J. Am. Chem. Soc.* **2017**, *139*, 7004.

(30). (a) Boronat, M.; Concepción, P.; Corma, A.; González, S.; IIIas, F.; Serna, P. *J. Am. Chem. Soc.* **2007**, *129*, 16230; (b) Zhang, S.; Chang, C. R.; Huang, Z. Q.; Li, J.; Wu, Z.; Ma, Y.; Zhang, Z.; Wang, Y.; Qu, Y. *J. Am. Chem. Soc.* **2016**, *138*, 2629; (c) Li, X. H.; Cai, Y. Y.; Gong, L. H.; Fu, W.; Wang, K. X.; Bao, H. L.; Wei, X.; Chen, J. S. *Chem. Eur. J.* **2014**, *20*, 16732.

(31). Studt, F.; Sharafutdinov, I.; Abild-Pedersen, F.; Elkjær, C. F.; Hummelshøj, J. S.; Dahl, S.; Chorkendorff, I.; Nørskov, J. K. *Nat. Chem.* **2014**, *6*, 320.

(32). (a) Shimizu, K.; Miyamoto, Y.; Kawasaki, T.; Tanji, T.; Tai, Y.; Satsuma, A. *J. Phys. Chem. C* **2009**, *113*, 17803; (b) Shimizu, K.; Miyamoto, Y.; Satsuma, A. *J. Catal.* **2010**, *270*, 86.

(33). (a) Stemmler, T.; Westerhaus, F. A.; Surkus, A.-E.; Pohl, M.-M.; Junge, K.; Beller, M. *Green Chem.* **2014**, *16*, 4535; (b) Stemmler, T.; Surkus, A.-E.; Pohl, M.-M.; Junge, K.; Beller, M. *ChemSusChem* **2014**, *7*, 3012.

(34). (a) Chen, F.; Topf, C.; Radnik, J.; Kreyenschulte, C.; Lund, H.; Schneider, M.; Surkus, A.; He, L.; Junge, K.; Beller, M. *J. Am. Chem. Soc.* **2016**, *138*, 8781; (b) Maki-Arvela, P.; Hájek, J.; Salmi, T.; Murzin, D. Yu. *Appl. Catal.* A **2005**, *292*, 1; (c) Li, Y.; Yu, S.; Wu, X.; Xiao, J.; Shen, W.; Dong, Z. Gao. J. *J. Am. Chem. Soc.* **2014**, *136*, 4031.

(35). (a) Mukherjee, S.; Zhou, L.; Goodman, A. M.; Large, N.; Ayala-Orozco, C.; Zhang, Y.; Nordlander, P.; Halas, N. J. *J. Am. Chem. Soc.* **2014**, *136*, 64; (b) Mukherjee, S.; Libisch, F.; Large, N.; Neumann, O.; Brown, L. V.; Cheng, J.; Lassiter, B.; Carter, E. A.; Nordlander, P.; Halas, N. J. *Nano Lett.* **2013**, *13*, 240; (c) Li, X. H.; Baar, M.; Blechert, S.; Antonietti, M. *Sci. Rep.* **2013**, *3*, 1743; (d) Hammer, B.; Nørskov, J. K. *Adv. Catal.* **2000**, *45*, 71; (e) García-García, F. R.; Bion, N.; Duprez, D.; Rodríguez-Ramos, I.; Guerrero-Ruiz, A. *Catal. Today* **2015**, *259*, 9.

(36). (a) Mikovksy, R. J.; Boudart, M.; Taylor, H. S. *J. Am. Chem. Soc.* **1954**, *76*, 3814; (b) Fujitani, T.; Nakamura, I.; Akita,T.; Okumura, M.; Haruta, M. *Angew. Chem. Int. Ed.* **2009**, *48*, 9515.

(37). O'Brien, C. P.; Miller, J. B.; Morreale, B. D.; Gellman, A. J. *J. Phys. Chem. C* **2011**, *115*, 24221.

(38). (a) Li, J.; Dickson, R. M.; Ziegler, T. *J. Am. Chem. Soc.* **1995**, *117*, 11482; (b) Huhmann-Cincent, J.; Scott, B. L.; Kubas, G. J. *J. Am. Chem. Soc.* **1998**, *120*, 6808.

(39). Niu, S.; Hall, M. B. *Chem. Rev.* **2000**, *100*, 353.

(40). (a) Serna, P.; Corma, A. *ACS Catal.* **2015**, *5*, 7114; (b) Serna, P.; Concepción, P.; Corma, A. *J. Catal.* **2009**, *265*, 19.

1
2
3
4
5
6
7
8
9
10
11
12
13
14
15
16
17
18
19
20
21
22
23
24
25
26
27
28
29
30
31
32
33
34
35
36
37
38
39
40
41
42
43
44
45
46
47
48
49
50
51
52
53
54
55
56
57
58
59
60

Insert Table of Contents artwork here

1
2
3
4
5
6
7
8
9
10
11
12
13
14
15
16
17
18
19
20
21
22
23
24
25
26
27
28
29
30
31
32
33
34
35
36
37
38
39
40
41
42
43
44
45
46
47
48
49
50
51
52
53
54
55
56
57
58
59
60

65x42mm (300 x 300 DPI)